Ferrite precipitation in quaternary Fe–C–X1–X2 systems using high-throughput approaches

Imed-Eddine Benrabah, H.P. van Landeghem, F. Bonnet, Benoît Denand, Guillaume Geandier, Alexis Deschamps

Ferrite precipitation in quaternary Fe-C-X1-X2 systems using high-throughput approaches

I.-E. Benrabah[a,b], H.P Van Landeghem[b], F. Bonnet[c], B. Denand[a], G. Geandier[a], A. Deschamps[b]

[a]Institut Jean Lamour, UMR CNRS-Université de Lorraine 7198, F-54000 Nancy, France. [b]Univ. Grenoble Alpes, CNRS, Grenoble INP, SIMAP, F-38000 Grenoble, France. [c]ArcelorMittal Research, F-57280 Maizières-lès-Metz, France.

Abstract

This study investigates the effect of composition on ferrite growth kinetics in quaternary Fe-C-X_1-X_2 systems (X: Ni, Cr, Mo) using a high-throughput methodology. This study provides the largest dataset to date on ferrite growth kinetics in multi-component steels, offering novel insight into the behavior of these complex systems. To this end, high-energy X-ray diffraction is utilized to gather kinetic data in situ along composition gradients, leading to the measurement of phase transformation kinetics maps in compositional space. The obtained data is compared to predictions from various models describing ferrite growth kinetics in low-alloy steels. The modified "three-jump" solute drag model is shown to describe best the ferrite growth kinetics in these quaternary systems, without the need for additional calibration or fitting parameters. The success of this model is attributed to its consideration of individual solute interactions with the interface and inter-elemental interactions. The findings of this study provide valuable insight for robust modeling of phase transformations and microstructural evolution in multi-component steels, a critical tool in accelerating alloy optimization and in enhancing process control.

***Keywords**:* Combinatorial metallurgy, Graded steels, High-throughput methodology, Ferrite growth kinetics, Solute drag

---

1. Introduction

Ferrite formation from austenite in steels is a longstanding research question that interested the scientific community for several decades [1, 2, 3, 4, 5]. The importance of this phase transformation in controlling the final mechanical properties of steels (such as dual phase and third generation advanced high strength steels (AHSS)) explains the attention this phenomenon has received. Over the years, different theories were proposed to describe the thermodynamics that govern austenite decomposition into ferrite [2]. The classical models such as para-

equilibrium (PE) and local-equilibrium (LE) were initially proposed to describe the phase transformation [2, 6, 1, 7, 8, 3]. However, it is now well documented that these two models are not suitable to describe ferrite growth kinetics in alloyed steels [9, 10, 11, 12]. Some of the experimental results showed that the measured kinetics can be slower than the predicted ones using PE and LE [9, 13]. This additional dissipation of the driving force was explained by two main factors, the intrinsic interface mobility [14, 15] and solute drag (SD). The latter effect (SD effect) was initially proposed by Cahn et al.[16]. It is based on the assumption that, during ferrite growth, solutes diffuse across the moving interface and dissipate a part of the available driving force. Odqvist et al. [17], Zurob et al. [18] and Chen et al. [19] proposed different numerical models to describe ferrite growth kinetics based on the SD effect. Recently, the authors [12] modified the original 'three-jump' solute drag model put forth by Zurob et al. [18] and tested its validity on different ternary Fe-C-X systems (X: Ni, Mn, Si, Cr and Mo) at different temperatures and on a large set of compositions [13, 20]. The results of the experiment, which involved measuring the growth kinetics of ferrite as a function of composition and temperature, showed a good match with the predictions of the solute drag model. This demonstrated that the model was able to accurately capture the amount of energy dissipated during the ferrite growth process. Additionally, the model's predictions for the concentration of solutes (X) at the γ/α boundary were consistent with experimental observations.

A natural next step for the present model would be to analyze the growth of ferrite in systems that contain multiple substitute elements. The segregation behavior of these elements at the interface would be more intricate in such systems, and the simultaneous presence of multiple solutes may alter their individual interactions with the moving interface. This is called the Coupled-Solute drag effect [21, 22, 23, 24]. These different interactions must be taken into account when modeling such complex systems. As it was shown by Guo and Enomoto [25], considering the attractive interaction between manganese and silicon enhances the dissipated drag energy in a Fe-C-Mn-Si alloy, resulting in even slower growth kinetics of ferrite. Moreover, carbon is reported to strongly segregate at the interface [26]. Thus, it is also important to consider the solute-carbon interaction that can be different between the two X_1 and X_2 solutes. Qiu et al. [23] used the initial version of the 'three-jump' model to predict ferrite growth kinetics in the Fe-C-Mn-Si quaternary system during decarburization experiments at different temperatures. The binding energies used for manganese and silicon, as well as the diffusion coefficients, were the same used to

successfully predict the growth kinetics in Fe-C-Mn and Fe-C-Si systems. Under all the studied conditions (different manganese and silicon contents and different temperatures), the predicted ferrite growth kinetics were slower than the measured ones. One of the suggested explanations to this result was the role of carbon on the segregation behavior of silicon and manganese at the interface. The different Mn-C (attractive) and Si-C (repulsive) interaction behaviors can change the segregation of the different elements to the interface and alter their 'effective' binding energies. Sun et al. [27] used the same approach to investigate ferrite growth kinetics in the Fe-C-Mn-Mo system. The authors cleverly chose this system where both Mn and Mo have attractive interactions with carbon, and thus one should expect that the effect of carbon is not apparent as in the Fe-C-Mn-Si system. The authors successfully predicted the growth kinetics in the Fe-C-Mn-Mo system using the solute drag parameters tuned on the respective ternary systems. The authors concluded their study by highlighting that: "Care needs to be taken in identifying the intrinsic binding energies of solutes (both substitutional and carbon) to the migrating interfaces".

In the recent version of the 'three-jump' solute drag model [12], the interaction between solutes was treated individually as suggested by the above cited studies. First, the carbon interaction with the interface was modified to capture the measured segregation levels in the steels. Second, the X-C and X_1-X_2 interactions were chosen so as to obtain Wagner coefficients in the interface equal to those in austenite. This last version of the SD model was validated experimentally on a large dataset of kinetics obtained on variable compositions in different Fe-C-X ternary systems and at different temperatures [20]. This was made possible using a newly developed high-throughput methodology combining compositionally graded materials and high-energy X-ray diffraction [13]. The methodology involves conducting in situ, space-resolved synchrotron X-ray diffraction measurements on samples with varying compositions. This allows for mapping the growth kinetics of ferrite as the composition changes. With this method, large amounts of data can be obtained through a limited number of experiments. The high-throughput approach has the potential to speed up the development of models and overall alloy design by rapidly exploring a broad range of compositions, as compared to traditional discrete experimental methods.

The objective of the present study is to use the same combinatorial approach [13] to study the effect of composition on ferrite growth kinetics in different quaternary Fe-C-X_1-X_2 systems (where X_1 and X_2 are Ni, Cr and Mo). Further, the obtained results will be compared with the new version of the solute drag model to validate it using this unprecedented dataset of ferrite

precipitation kinetics across a wide range of alloy compositions.

2. Experimental procedure

2.1. Materials

The alloys used in the present work were provided by ArcelorMital Research SA, and their chemical composition is listed in table 1.

Table 1: The chemical compositions (wt.%) of the alloys used to create the graded samples.

Composition (wt. %)	C	Mn	Si	Mo	Cr	Ni	Other alloying elements	Ae_3 (°C)
Fe-C-Mo	0.26	0.004	0.02	0.21	<0.002	<0.002	<0.002	823
Fe-C-Ni	0.26	0.002	0.03	<0.002	<0.002	0.98	<0.002	795
Fe-C-Cr	0.26	0.004	0.02	<0.002	1.0	<0.002	<0.002	823

2.2. The high-throughput methodology

The graded samples Fe-C-X_1-X_2 were created from homogeneous ternary samples Fe-C-X_1 and Fe-C-X_2 (listed in table 1), where X_1 and X_2 are substitutional elements (Ni, Mo or Cr). The methodology used to fabricate the diffusion couples was already detailed in a previous study [13] and only a summary is given below.

First, the two iso-composition samples (Fe-C-X_1 and Fe-C-X_2) are joined together in the solid-state using uniaxial hot compression. Then, high temperature diffusion heat treatments are used to create the desired composition gradients. Finally, the grain size is controlled using cyclic heat treatments and plastic deformation. Electron probe micro-analysis (EPMA) was used to measure the obtained composition gradients along the diffusion couples. An energy of 15 kV and a probe current of 900 nA were used on a CAMECA SX50 electron micro-probe. For quantitative carbon measurements, standards containing different known carbon compositions were used to calibrate the C Kα intensity.

Once the diffusion couples are created, the next step is to acquire the evolution of ferrite fraction as a function of time and composition through high energy X-ray diffraction (HEXRD). This in-situ HEXRD was performed on the P21.2 beamline at the DESY synchrotron (Hamburg, Germany) using PETRA III. The experimental parameters are summarized in table 2. Samples, measuring 3 mm in diameter and 30 mm in length were cut from the graded samples and heat-treated in a

custom lamp furnace with a rotary sample holder to allow maximizing the number of orientations in the diffracting volume of each pattern. The details of the applied heat treatments were as follows: first, samples were heated up to 910 °C and held for 30 s to ensure a single-phase austenitic microstructure. The samples were then rapidly cooled to the intercritical (α + γ) domain (730 °C, 750 °C and 775 °C) and held for 15 min before a final gas quench to room temperature. To analyze the phase transformation along the gradient of composition during the heat treatments, the samples were translated vertically at a 1 $mm.s^{-1}$ speed using the beamline motor. With an acquisition rate of 10 Hz, this resulted in a time resolution of 6 to 22 s (depending on the composition length) for each composition along the composition gradient and a space (compositional) resolution of ∼150 µm (corresponding to 0.02 to 0.05 wt.% composition resolution for a 6 mm and 2 mm gradient length, respectively). Debye-Scherer rings were collected in transmission mode and were integrated using the pyFAI software package [28]. The volume fractions of the various phases were calculated using the Rietveld method, as implemented in the FullProf software package. [29].

Table 2: The different parameters used during HEXRD experiments.

Energy (keV)	Wave length (Å)	Beam size	Detector	Acquisition rate (Hz)	Distance detector sample (m)
82	0.1512	1 mm x 80 µm	VAREX detector 4343CT	10	~ 1

3. Phase transformation modeling

An important feature of the present methodology is that the generated data set can be used to validate the different models developed to describe the ferrite growth kinetics as a function of solute content. In the present contribution, three different models based on different assumptions were compared to the experimental results, named LE, PE and SD. Local equilibrium (LE) and Para-equilibrium (PE) calculations were carried using ThermoCalc with the TCEF9 and Mob2 databases [30]. It is important to note that the nucleation effect was not considered in this study. The nucleation sites were assumed to be saturated during the early stages of the phase transformation. Such site saturation was assumed in other studies for similar conditions [31, 32]. To illustrate this point, Figure S1 in the supplementary materials shows an optical micrograph of

the Fe-C-Ni-Mo diffusion couple heat treated at 750 °C for 30s, where it can be observed that ferrite has covered all the prior austenite grain boundaries. However, for a finer description of the overall austenite to ferrite phase transformation, nucleation should be included in subsequent SD models. Another important factor is the grain geometry, assumed here to be spherical as suggested in the literature [33]. Thus, the effect of both nucleation and the grain geometry on the overall transformation kinetics is out of the scope of the present work and the assumptions commonly found in the literature were kept for simplicity's sake.

The third model used in this contribution is the so called 'three-jump' solute drag (SD) model, initially developed by Zurob et al. [18] and recently modified by the present authors [12]. It describes the movement of solute across the interface between ferrite and austenite in a discrete way, with three separate steps or "jumps" involved: from ferrite to the interface, within the interface, and from the interface to austenite. Each of these jumps has its own diffusion coefficient. Ferrite growth is assumed to be controlled by carbon diffusion in austenite. The carbon content in austenite and ferrite are calculated from the energy balance between the driving chemical energy and the dissipated energy due to solute drag. One of the main modifications in the updated version of the SD model is the consideration of not only the interaction of the solute element with the interface but also the interaction of carbon with the interface and the interaction between the different elements (C-X and X_1-X_2). The friction energy is neglected in the SD model. More details about the SD model and its modifications can be found in [12, 18].

The SD model includes one fitting parameter, which represents the interaction energy between the substitutional element (X) and iron (Fe) at the interface. This parameter is described using the $L_{Fe,X:Va;0}$ parameter of the ThermoCalc database and it will be here referred to as Fe-X, for simplicity. It has been demonstrated that this parameter can be associated with the binding energy (E_0) [12]. In a recent contribution [20], the present SD model was used to study ferrite growth kinetics in various ternary Fe-C-X systems (X: Ni, Mn, Mo, Si and Cr) using the high-throughput methodology. It was found that the model was able to accurately predict the measured kinetics using only the single Fe-X interaction parameter as a fitting parameter. This parameter was shown to be independent of solute composition but dependent on temperature in certain cases (as for the Fe-C-Si system). The objective of the present study is first to extend the SD model to quaternary systems and second, to test if the same fitted parameters on two ternary systems, Fe-C-X_1 and Fe-

C-X_2, can be used to predict the growth kinetics in the corresponding quaternary Fe-C-X_1-X_2 systems without any further fitting parameters.

4. Results

Three quaternary Fe-C-X_1-X_2 systems were investigated in the present contribution as summarized in table 3. All the studied temperatures are shown in the same table for each system. Figure 1 shows an example of the obtained gradients in a diffusion couple between Fe-C-Ni and Fe-C-Mo samples. The diffusion couple contains opposite gradients of nickel and molybdenum ranging from 0 %Ni (resp. 0.2 % Mo) to 1%Ni (resp. 0% Mo) over a distance of 3 mm. A gradient of carbon was measured along the diffusion couple (0.18 % wt. at the nickel rich side and 0.2 % wt. at the molybdenum rich side). The gradient lengths for the other diffusion couples are shown in table 3, as well as the associated carbon content. Two other important parameters should be taken into account in modeling: the exact temperature and the exact grain size.

The grain size was measured at the end of the transformation along the graded samples using optical metallography and was assumed to evolve linearly between the gradient extremities. For the temperature gradient, previous estimation on the ternary alloys indicated temperature gradients of ~1.6 °C.mm^{-1} [12]. This was assumed to hold for the present samples as all the experiments were realized during the same experimental run. These parameters are also included in Table 3.

Table 3: Details concerning the applied heat treatment, including the austenitization and the isothermal holding temperatures. It also displays the length of the measured composition gradient, carbon concentration, temperature, and grain size measured along the gradient.

Diffusion couple	T_γ	T_{iso}	Gradient length (mm)	Carbon content (wt. %)	Temperature gradient (°C/mm)	Grain size (μm) [±10]
Fe-C-Ni/Fe-C-Mo	910°C	730°C 750°C 775°C	3.5	0.18-0.2	1.6	50
Fe-C-Ni/Fe-C-Cr	910°C	750°C 775°C	5.5	0.2	1.6	40 - 90
Fe-C-Cr/Fe-C-Mo	910°C	750°C 775°C	1.6	0.25	1.6	40-60 @ 750°C 60-75 @ 775°C

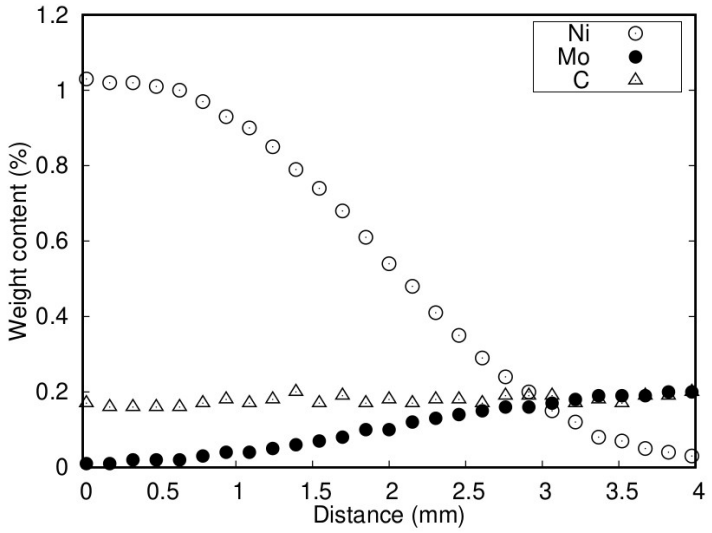

Figure 1: Nickel, molybdenum, and carbon contents across the diffusion couple between Fe-C-Ni and Fe-C-Mo samples, as measured using EPMA.

2.1. Fe-C-Ni-Mo system

The evolution of ferrite fraction as function of time, nickel and molybdenum contents is shown in figure 2-a, b and c for the three temperatures, 730 °C, 750 °C and 775 °C. Each curve represents the growth kinetics of ferrite with a specific combination of nickel and molybdenum content at a specific temperature. For a beam size ranging from 80 to 120 µm, each curve represents a maximum variation in nickel and molybdenum content of approximately 0.025% and 0.005%, respectively. Ferrite growth slows down with increasing nickel content (resp. decreasing molybdenum content) and with increasing temperature.

Figures 2-d, e and f compare the compare the predicted final ferrite fractions from the LE and PE models with the experimentally measured values as a function of nickel and molybdenum content for three different temperatures: 730 °C, 750 °C and 775 °C, respectively. The effect of nickel and molybdenum composition is more noticeable at higher temperatures. The ferrite fraction formed at the end of the isothermal hold at 775 °C ranges from 55 % on the molybdenum-rich side to 9 %

on the nickel-rich side. For the three temperatures, the PE model fails to predict the measured values. The gap between measurements and PE predictions increases with increasing nickel content (i.e. decreasing molybdenum content) and increasing temperature. For the LE model, this differs for each temperature. At 730 °C, the estimated ferrite fractions using the LE model are somewhat greater than the actual ones across the entire range of nickel/molybdenum composition. A consistent discrepancy is observed between the measured and the predicted LE fractions, with the latter being around 3 to 5 % higher.

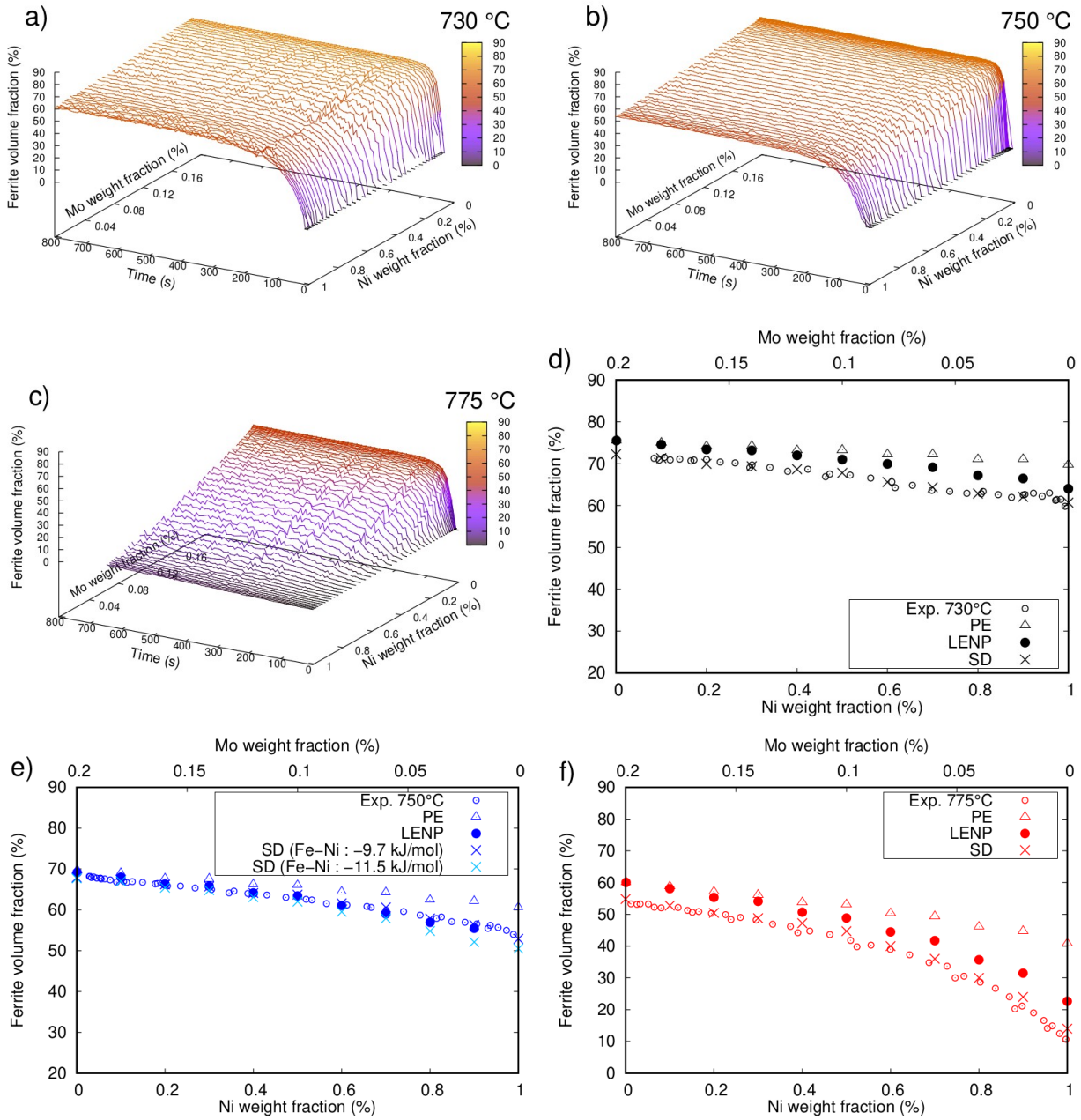

Figure 2: Comparison of measured and predicted ferrite fractions in Fe-C-Ni-Mo alloys at different temperatures. Sub-figures (a-c) show the progression of ferrite fraction measured using high energy X-ray diffraction (HEXRD) as a function of time and the composition of nickel and molybdenum along the Fe-C-Ni-Mo diffusion couple during isothermal holding at three different temperatures (730°C, 750°C, and 775°C). Sub-figures (d-f) compare the measured final ferrite fractions (represented by open circles) with the predictions of PE (represented by triangles), LENP (represented by filled dots), and solute drag (represented by crosses) models as a function of nickel content at the three temperatures respectively.

The measurements and the predictions made by the LE model at 750 °C show good agreement throughout the entire composition range. However, at 775 °C, the LE model fails to predict the final ferrite fraction reached at the end of the isothermal hold for all nickel/molybdenum compositions, and the discrepancy between the LE calculations and measurements grows with increasing nickel content. The comparison of the experimental results with the SD predictions is also shown in Fig.2-d to f. As a first attempt, the Fe-Ni and Fe-Mo, (or Fe-X_1 and Fe-X_2 for other systems) interaction parameters were gathered from the results of the solute drag modeling of the ternary Fe-C-Ni and Fe-C-Mo systems already presented in [13]. For the 730 °C temperature, this corresponds to -11.7 kJ.mol^{-1} and -7 kJ.mol^{-1}, respectively. The calculated ferrite fractions, obtained through the use of these parameters, match well with the measured ones. The same observation can be made for the 775 °C case, where the calibrated ternary Fe-Ni (-11.9 kJ.mol^{-1}) and Fe-Mo (-8 kJ.mol^{-1}) interaction parameters, accurately represents the measured ferrite fraction as a function of nickel and molybdenum content.

At 750 °C and using the same Fe-X interaction parameters obtained from the previous study (Fe-Ni = -11.8 kJ.mol^{-1} and Fe-Mo = -7.5 kJ.mol^{-1}), the SD model predicts well the final ferrite fraction up to 0.5Ni-0.1Mo (wt.%) and then slightly underestimates the measured value on the nickel rich side. By adjusting the Fe-Ni to -9.7 kJ.mol^{-1}, a better fit is obtained over the whole range of composition.

We will now compare the differences between the measured progression of ferrite fraction over time during the isothermal holding process as obtained through HEXRD experiments and the theoretical values estimated by three models. Figure 3 shows a full comparison of the experimental kinetic maps in (time, Ni/Mo composition) space with the PE, LE and SD model predictions at the 750 °C temperature. The predicted kinetics from both the LE and PE models are found to be faster than the actual values across the entire range of nickel/molybdenum composition, as observed at the temperature under consideration. The SD model shows a better, but not perfect description of the growth kinetics at this temperature. For a more quantitative comparison, individual growth kinetics of two selected nickel and molybdenum compositions (0.4 %Ni-0.12 %Mo and 0.7%Ni-0.06%Mo) are compared with the predictions of the different models at the three temperatures, 730 °C, 750 °C and 775 °C (figure 4). PE predicts faster ferrite growth than observed for all shown conditions (i.e. nickel and molybdenum compositions and temperatures). The LE model predicts kinetics slower than the PE model but still quicker than the

observed ones. Even in cases where the LE model succeeds in predicting the final fractions, the predicted transformation rate does not match the experimental record as shown in figures 4-b and 4-e. The SD model returns a better description of the evolution of ferrite fraction as a function of time for the different conditions. To be noted that the agreement was obtained using the above-mentioned Fe-Ni and Fe-Mo fitting parameters (Fe-Ni : -11.8 kJ.mol^{-1} and Fe-Mo : -8 kJ.mol^{-1}).

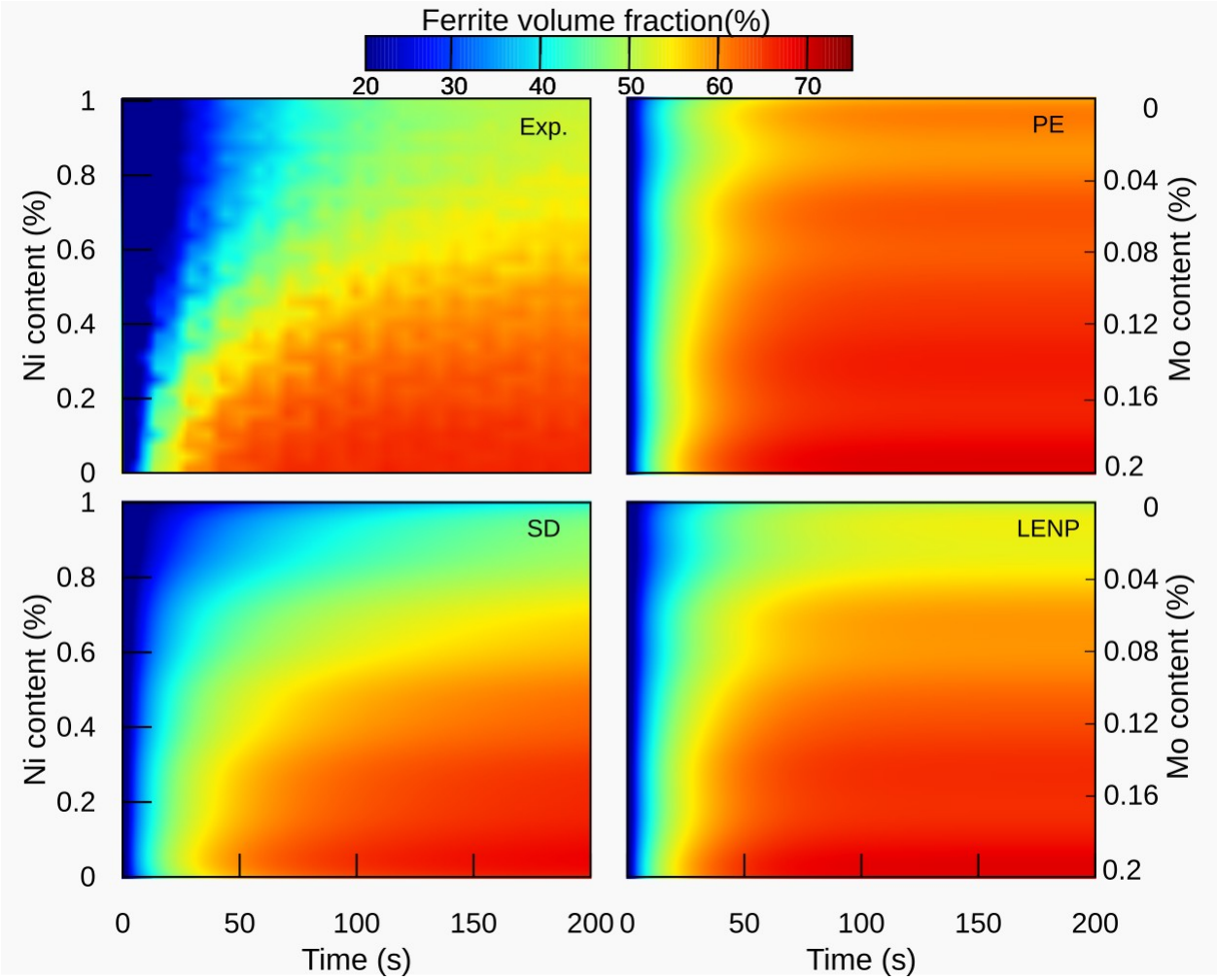

Figure 3: 2D representation of the ferrite growth kinetics during the isothermal holding at 750°C based on time and Ni/Mo composition. The experimental results (Exp.) are compared with the prediction of the different models, para-equilibrium (PE), local equilibrium with no partition (LENP) and solute drag (SD). The SD calculations were realized using Fe-Ni = -9.7 kJ.mol^{-1} and Fe-Mo = -7.5 kJ.mol^{-1}.

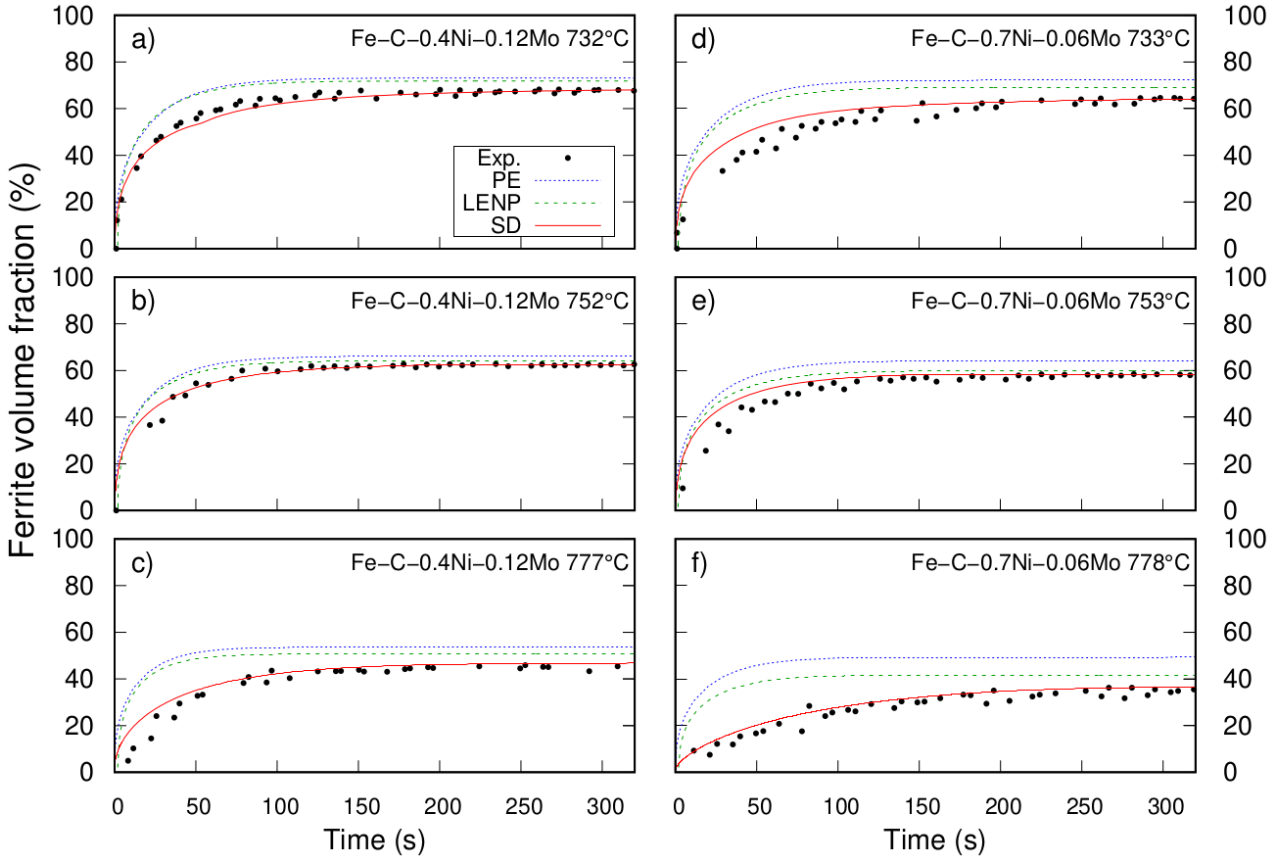

Figure 4: Measured ferrite growth kinetics, obtained through HEXRD experiments in the Fe-C-Ni-Mo diffusion couple during the isothermal holding, for two different compositions: Fe-0.19C-0.4Ni-0.12Mo (%wt.) at : a) 732 °C, b) 752 °C and c) 777 °C. and Fe-0.19C 07Ni-0.06Mo (%wt.) at: d) 733 °C, e) 753 °C and f) 778 ◦ C. The kinetics predicted by the PE, LE, and SD models are displayed for various compositions.

2.2. Fe-C-Ni-Cr system

The evolution of ferrite fraction as a function of time, nickel and chromium contents is shown in figure 5-a and b for the two temperatures, 750 °C and 775 °C. It can be observed that both the ferrite growth kinetics and the final ferrite fraction decrease with increasing chromium content (i.e. decreasing nickel content) and with increasing temperature. The important grain size difference noticed along the graded sample (90 µm on the chromium rich side and 40 µm on the nickel rich side), may also contribute to the observed growth kinetics.

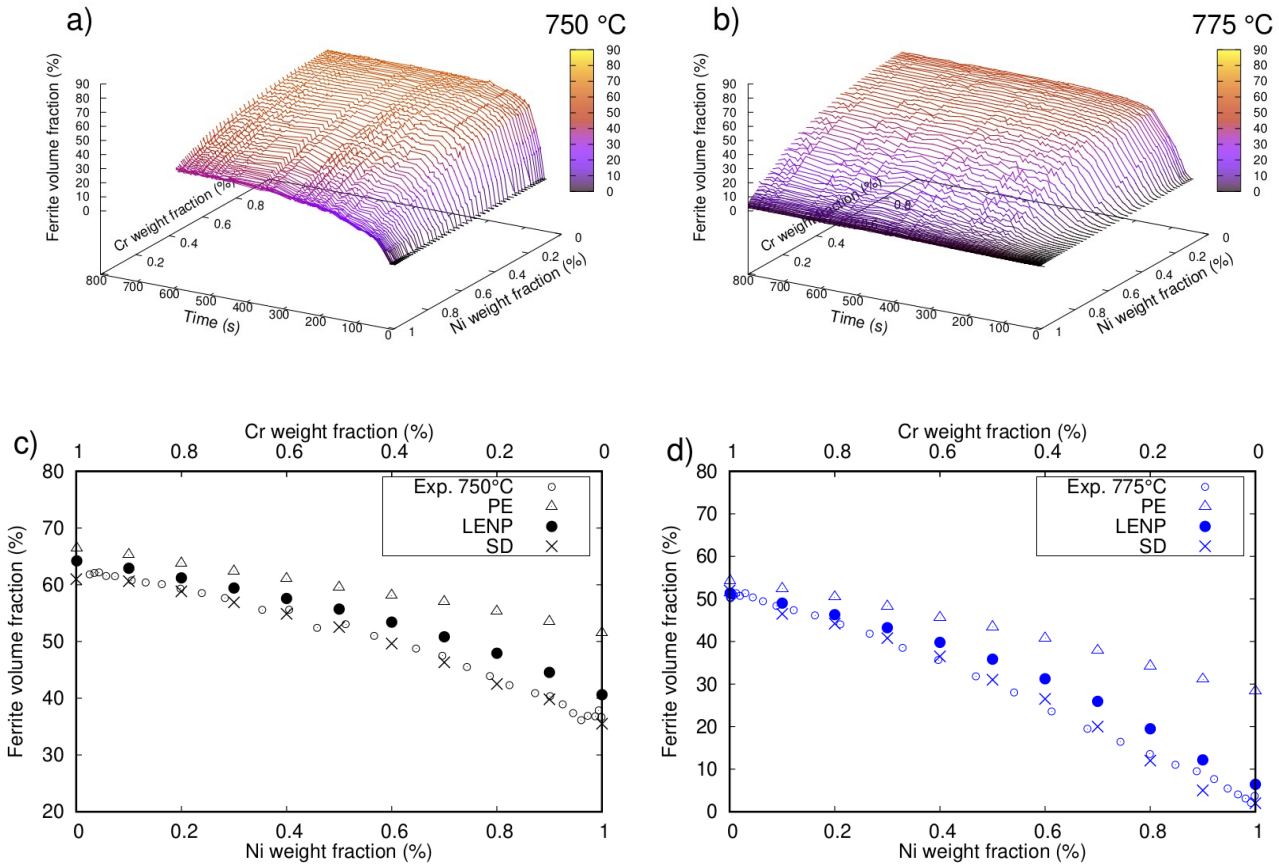

Figure 5: The evolution of the ferrite fraction in the Fe-C-Ni-Cr diffusion couple during an isothermal hold at two temperatures, 750 °C and 775 °C, as determined using HEXRD. Sub-figures a) and b) show the change in ferrite fraction over time for different nickel and chromium compositions. Sub-figures c) and d) compare the final measured ferrite fractions (represented by open circles) to the predictions made by the PE (triangles), LENP (filled dots), and SD (crosses) models in relation to nickel and chromium content at each temperature.

The final amount of ferrite that was formed after the isothermal hold is displayed in the figure 5-c and d as a function of nickel and chromium contents and for the two studied temperatures. In the same figure are plotted the predicted ferrite fractions under the same conditions using PE, LE and SD models. The overall kinetics of individual Ni/Cr contents are plotted in figure 6 for different temperatures and compared to the calculated growth kinetics using the three models. The PE model overestimates the measured fractions in all the studied conditions. The gap between measurements and the predictions of the PE model increases with increasing nickel content and with increasing temperature. At 750 °C, the LE model predicted final ferrite fractions are much closer to the measurements especially at the chromium rich side (a relative difference of 3 % at the chromium rich side). The discrepancy between LE predictions and measurements increases with increasing nickel content to reach a relative difference of 8 % at the nickel rich side.

However, it can clearly be noticed that LE overestimates the growth rate (figure 6-a, b and c). At 775 °C, the predicted LE final fractions are in good agreement with the measurements on the chromium rich side and start diverging from the measured fractions with increasing nickel content. This model, however, also predicts faster transformation kinetics than the experimental observations over the whole range of composition (figure 6-d, e and f).

Finally, the SD model shows good agreement with the obtained measurements for both temperatures and over the whole range of Ni/Cr composition. This is true for both the final ferrite fractions and the growth kinetics. It should be noted that the Fe-Ni and Fe-Cr parameters used here were the same as used for the ternary Fe-C-Ni and Fe-C-Cr systems for 750 °C [20] (i.e. -11.8 $kJ.mol^{-1}$ and +5.3 $kJ.mol^{-1}$, respectively). For 775 °C, we used the same Fe-Ni interaction parameters (11.9 $kJ.mol^{-1}$) as that used for the ternary system, however, no data was available for the ternary Fe-C-Cr system at this temperature [20]. As an alternative, the Fe-C-Cr was calibrated on the rich side of the current quaternary Fe-C-Ni-Cr system. The best fit was thus obtained using an Fe-Cr parameter of +6.1 $kJ.mol^{-1}$. Note that using the same Fe-Cr interaction parameter as for the 750 °C results in an underestimation of the final ferrite fraction by a 3 % absolute difference. This deviation is within acceptable range.

Figure 6 compares the experimental results of ferrite fraction as a function of time with the predictions of the PE and LE models for three nickel and chromium compositions, namely 0.2Ni-0.8Cr, 0.5Ni0.5Cr and 0.8Ni-0.2Cr, and at two different temperatures, 750 °C, 775 °C. Under all the studied conditions, the PE predicted growth kinetics are faster than the measurements at both temperatures. The LE predicted ferrite growth kinetics are also faster than the measured ones, even in cases where the final fractions predicted by the LE model are in agreement with the measurements, as shown in figure 6-d.

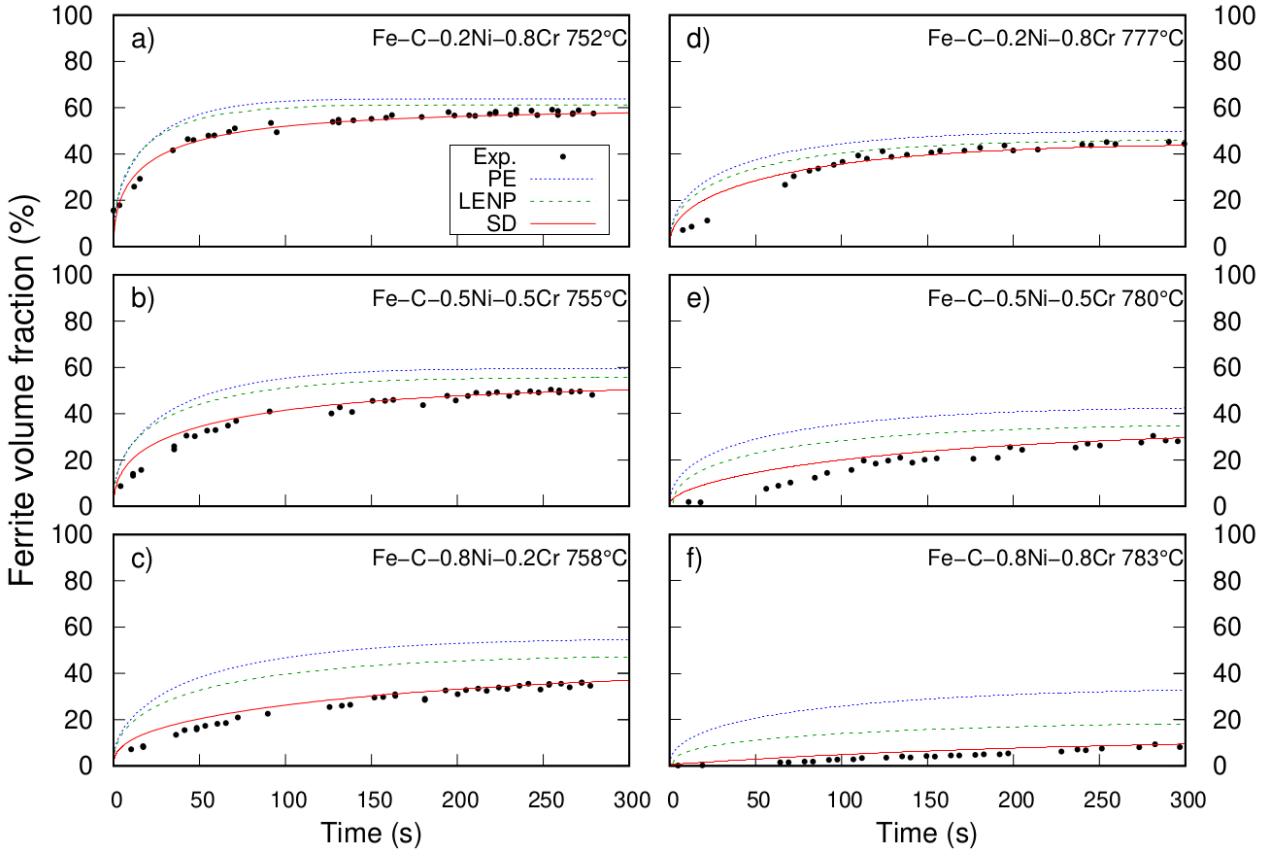

Figure 6: Comparison between the experimental and calculated ferrite fraction evolution as a function of time during the isothermal holding of the Fe-C-Ni-Cr diffusion couple, for the three compositions : Fe-0.2C-0.2Ni-0.8Cr (%wt.) at : a) 752 °C and d) 777 °C, Fe-0.2C-0.5Ni-0.5Cr (%wt.) at: b) 755 °C and e) 780 °C and Fe-0.2C-0.8Ni-0.2Cr (%wt.) at : c) 758 °C and f) 783 °C.

4.3. Fe-C-Cr-Mo system

The evolution of the ferrite fraction measured using HEXRD, as a function of time, chromium, and molybdenum content during the isothermal hold is displayed in figure 7-a and b for two temperatures, 750 °C and 775 °C. Figure 7-c and d show a comparison between the final ferrite fraction as a function of chromium and molybdenum contents, as measured by HEXRD experiments, and the predictions made by PE, LE, and SD models at two temperatures, 750 °C and 775 °C. The growth kinetics of the ferrite phase for selected chromium and molybdenum contents are compared to the predictions of the three models in figure 8 at both 750 °C and 775 °C.

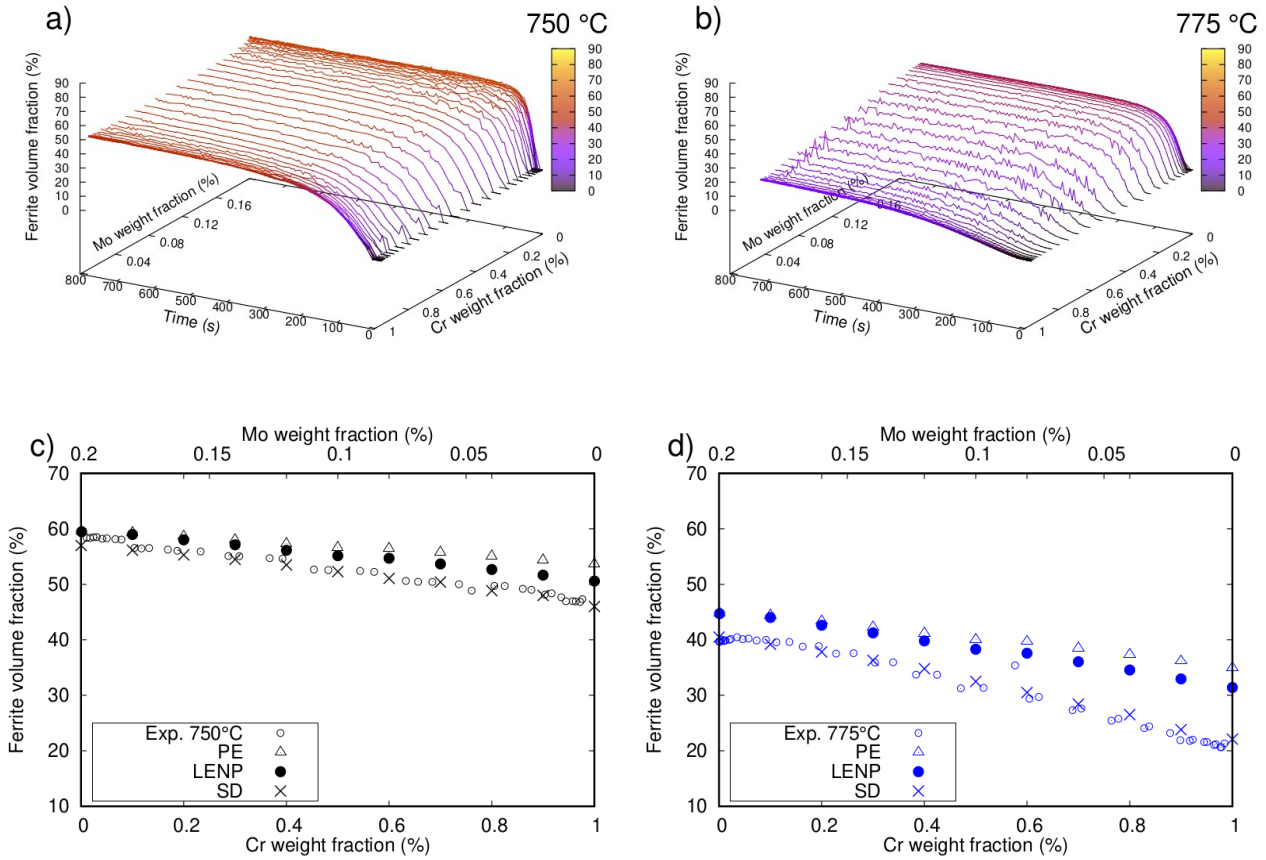

Figure 7: Evolution and comparison of ferrite fraction along the Fe-C-Cr-Mo diffusion couple. a) and b) Measured ferrite fraction using HEXRD as a function of time and chromium/molybdenum composition at 750 °C and 775 °C. c) and d) Comparison of measured final ferrite fractions (open circles) and predictions of PE (triangles), LENP (filled dots), and SD (crosses) models at 750 °C and 775 °C.

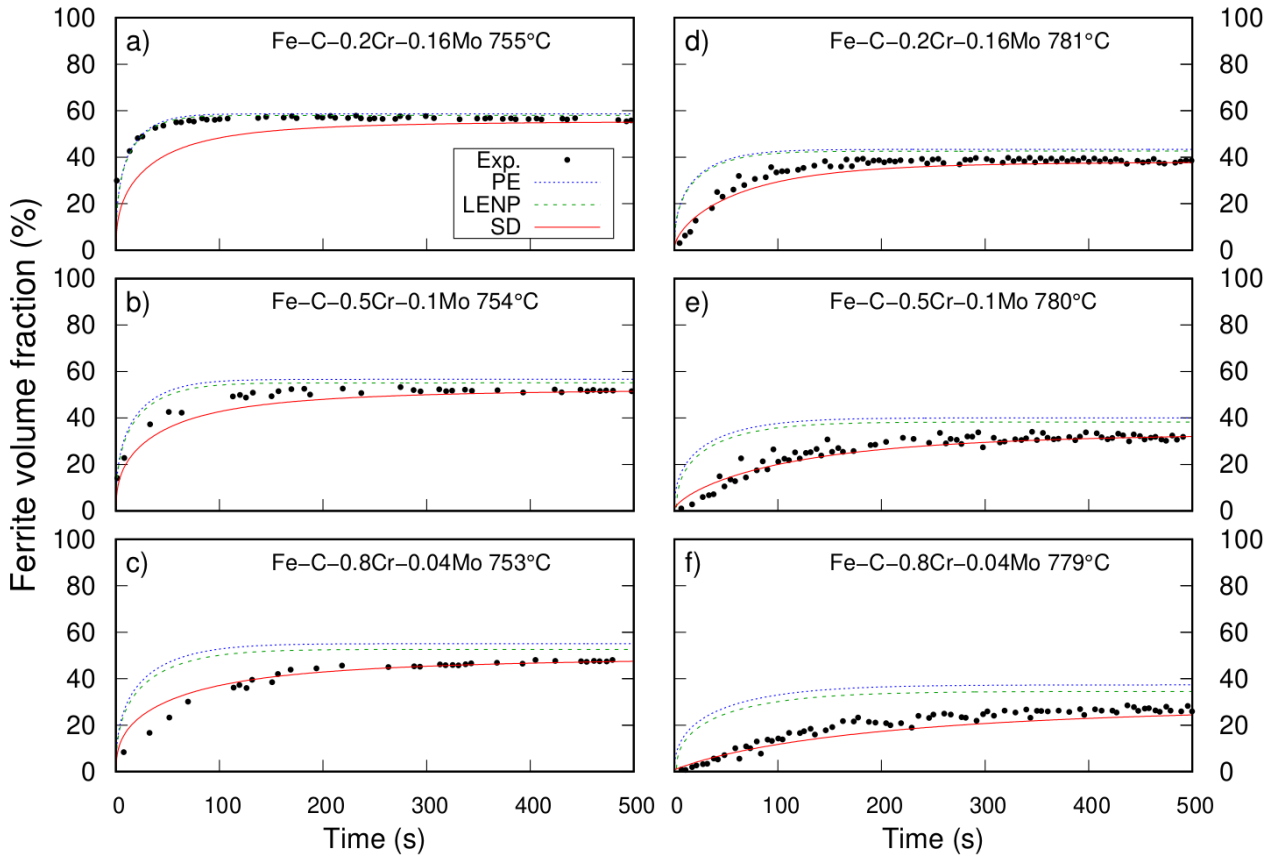

Figure 8: HEXRD-measured ferrite growth kinetics of Fe-C-Cr-Mo diffusion couple at different compositions and at different temperatures. Fe-0.52C-0.2Cr-0.16Mo (%wt.) at: a) 755 °C and d) 781 °C, Fe-0.25C-0.5Cr-0.1Mo (%wt.) at: b) 754 °C and e) 780 °C and Fe-0.26C-0.8Cr-0.04Mo (%wt.) at: c) 753 °C and f) 779 °C. PE, LE and SD model predictions also shown.

Results show that both PE/LE models predict faster kinetics than the measured ones at both temperatures and over the entire composition range, except for the molybdenum rich side of the graded sample treated at 750 °C. In this case, the PE/LE models accurately describe the measured ferrite growth kinetics, as seen in figure 8-a. The Solute Drag model accurately predicts the ferrite growth kinetics and final ferrite fractions for most of the studied Cr/Mo compositions and temperatures. At 750 °C, the SD model underestimates the growth kinetics for the Mo rich side. The same Fe-Mo interaction parameters that were used to model ferrite precipitation in the ternary Fe-C-Mo system were applied to predict ferrite growth kinetics in the quaternary Fe-C-Cr-Mo system at both temperatures. For modeling ferrite growth kinetics at 750 °C, the Fe-Cr interaction parameter was the same as for the ternary system. However, for 775 °C, the Fe-Cr interaction parameter was further adjusted using the ternary composition of the quaternary diffusion couple, resulting in a different value (+1.9 kJ.mol^{-1}) compared to the one used to model

ferrite growth kinetics in the Fe-C-Ni-Cr system at a similar temperature (+6.1 $kJ.mol^{-1}$). This significant difference in the Fe-Cr interaction parameter at 775 °C is surprising and one possible explanation is the carbon content difference between the two systems (0.2% and 0.26% for the Fe-C-Ni-Cr and Fe-C-Cr-Mo systems, respectively).

5. Discussion

In a previous contribution, we showed that the updated 'three-jump' solute drag model successfully predicts the evolution of ferrite as a function of time during isothermal holding for different Fe-C-X systems, for a relatively wide range of composition (0% to 1%) and at different temperatures. It was also shown that the fitting parameter (Fe-X interaction) used in the SD model, was independent of composition, but may show a dependency on temperature. The objective of the present contribution was to test the possibility to extend this SD model to higher order (quaternary) Fe-C-X_1-X_2 alloys, without the need for further fitting parameters.

The present results showed that the present version of the SD model was overall able to predict the ferrite growth kinetics of the quaternary Fe-C-X_1-X_2 systems using the same fitting parameters obtained from the ternary Fe-C-X_1 and Fe-C-X_2 systems. To further investigate the solute drag effect on ferrite growth kinetics, figure 9 displays an example of the energy dissipated due to nickel and molybdenum diffusion across the interface, as a function of the interface velocity, for the Fe-C-0.5-Ni-0.1Mo composition at 730 °C. This is a classical solute drag plot where the dissipated energy first rises as the interface velocity slows down, reaches a peak at intermediate velocities ($\sim 3.10^{-8}$ $m.s^{-1}$), then decreases when the velocity slows down even further. On the same figure are plotted the dissipated energies due to nickel diffusion and the one due to molybdenum diffusion across the interface. As the interface velocity decreases, the energy dissipated due to molybdenum diffusion starts at higher interface velocities compared to the energy dissipated due to nickel diffusion. This is due to the higher diffusion coefficient of molybdenum from ferrite to the first atomic plane of the interface (D_α Mo: $\sim 8.10^{-17}$ $m^2.s^{-1}$) compared to the one for nickel (D_α Ni: $\sim 3.10^{-17}$ $m^2.s^{-1}$). The energy dissipated due to nickel diffusion contributes more at lower velocities ($v < 1.10^{-9}$ $m.s^{-1}$).

In a previous study [23], the previous SD version failed to predict ferrite growth kinetics in the Fe-C-Mn-Si system using the same fitting parameters from the Fe-C-Mn and Fe-C-Si system. The

authors claimed that this can be related to the complex interaction between Mn, Si, C and the interface. Sun et al. [27] applied the same solute drag model to the Fe-C-Mn-Mo system, where both Mn and Mo have a positive interaction with carbon and were able to accurately predict the measured growth kinetics using Fe-X values calibrated from the ternary systems. Both studies highlighted the importance of taking into account the individual binding energies of solutes (both substitutional and carbon) to the α/γ interface.

If now we consider the presently studied systems, based on the relevant Wagner coefficients presented in table 4, different scenarios can be identified. Starting with the Fe-C-Ni-Mo system, molybdenum has a strong attractive interaction with carbon, while nickel has a repulsive interaction with carbon at the interface (similar to the Fe-C-Mn-Si system). The interaction between nickel and molybdenum is attractive in austenite while it is very weak in ferrite. The same X-C interaction behavior is expected for the Fe-C-Ni-Cr system, where chromium has an attractive interaction with carbon and nickel a repulsive interaction with carbon. Meanwhile, the interaction between chromium and nickel is weak in both phases. Finally, in the Fe-C-Cr-Mo system, both solutes have an attractive interaction with carbon at the interface, and a slightly repulsive interaction between Cr and Mo is expected in both bulk phases.

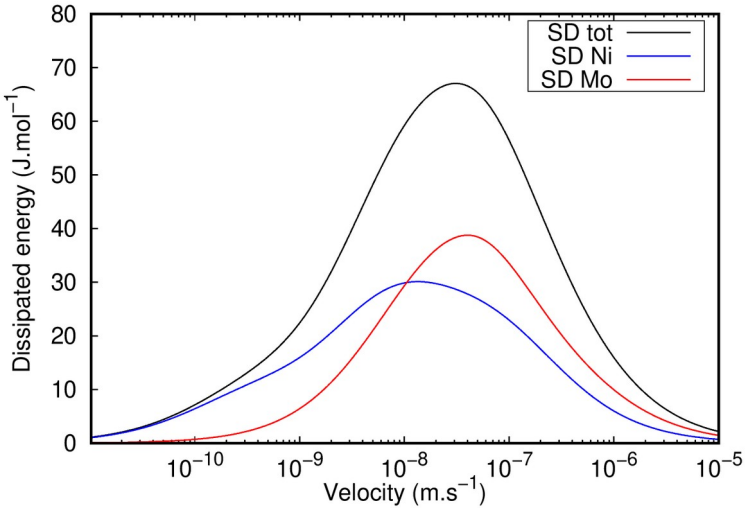

Figure 9: Dissipated energy from nickel and molybdenum diffusion across the interface vs. interface velocity for Fe-0.19C-0.5Ni-0.1Mo (wt.%) at 730 °C.

Table 4: The Wagner interaction parameters between Ni-Mo, Ni-Cr and Cr-Mo in both austenite and ferrite at the different temperatures, calculated using the ThermoCalc software [34].

Temperature (°C)	730		750		775	
$\epsilon_{X_1-X_2}$	Ferrite	Austenite	Ferrite	Austenite	Ferrite	Austenite
Ni-Mo	0.1	-6.5	0.1	-6	0.1	-5.3
Ni-Cr	-2	-0.1	-2	-0.1	-1.5	-0.1
Cr-Mo	2.2	3.3	2.1	3.3	2	3.1

For all the above-stated scenarios, a good match was found between the measured kinetics and the SD results, confirming the hypothesis that the complex interaction between the different elements and the interface should be taken individually as in the current version of the SD model. First, the carbon interaction with the interface (Fe-C) is modified here to capture the noticed high carbon segregation at α/γ interfaces, using the $L_{Fe:C,Va}$ interaction parameter in the ThermoCalc database. This parameter was set to -50 kJ.mol^{-1} for all the systems and thus is not a fitting parameter. Second, the solute interaction with the interface (Fe-X) was taken as the fitting parameter and is thus modified to capture the measured growth kinetics (in the ternary systems). This was done by modifying the $L_{Fe,X:Va}$ interaction parameter of the ThermoCalc database. Finally, the solute-carbon (X-C) and solute-solute (X_1-X_2) interaction parameters are assumed to be equal to the ones in austenite. To this end, the Wagner interaction parameters, ϵ_{XC} and ϵ_{X1X2}, were calculated using Eq.1 and Eq.2 in austenite and the $L_{Fe,X:C,Va}$ and $L_{Fe,X1,X2:Va}$ were modified in the interface using the same equations so that its Wagner interaction parameters are identical to austenite. This procedure was performed independently on the studied system and is not considered as an adjustable parameter. The detailed description of the parameters in ϵ_{XC} and ϵ_{X1X2} is given in [12]. It is worth emphasizing that, based on Eq.1 and Eq.2, the Wagner interaction parameter is function of both the $L_{Fe,X:Va}$ and $L_{Fe:C,Va}$ interaction parameter. This indicates that changing $L_{Fe,X:Va}$ alone only (as in previous implementations of the model) results in a change in the interaction behavior between solutes (X-C and X_1-X_2) at the interface.

$$\epsilon_{XC} = -\left\{\left(L^0_{Fe,X:Va} + L^1_{Fe,X:Va} + L^2_{Fe,X:Va}\right) + \left(L^0_{Fe:C,Va} - L^1_{Fe:C,Va} + L^2_{Fe:C,Va}\right) - \left(L^0_{X:C,Va} - L^1_{X:C,Va} + L^2_{X:C,Va}\right) - \left(L^0_{Fe,X:C}\right.\right. \quad (1)$$

$$\epsilon_{X1X2} = -\left\{\left(L^0_{Fe,X1:Va} + 2L^1_{Fe,X1:Va} + 3L^2_{Fe,X1:Va}\right) + \left(L^0_{Fe,X2:Va} + 2L^1_{Fe,X2:Va} + 3L^2_{Fe,X1:Va}\right) - \left(L^0_{X1,X2:Va}\right) - L_{Fe,X1,X2:Va}\right\} / RT \quad (2)$$

One important observation in the present study was the different Fe-Cr interaction parameters used to fit the data in the Fe-C-Cr-Mo and Fe-C-Cr-Ni systems at 775 °C. One possible explanation for this difference could be the different carbon contents in the two systems, but this would have also resulted in a different Fe-Cr interaction parameter at 750 °C, which was not observed. Another potential explanation is the use of the $L_{Fe:C,Va}$ interaction parameter, which was set to -50 kJ.mol^{-1} for all systems and temperatures in the study. This value was chosen based on the high carbon segregation at the α/γ interfaces as measured using the APT technique, but further investigation is needed to determine the precise value of this parameter and whether it varies with temperature. It is also possible that the discrepancy between the results could be due to an experimental error in the HEXRD experiments.

6. Conclusion

The high-throughput approach used in this study proved to be an effective method for investigating the impact of composition on ferrite growth kinetics in quaternary Fe-C-X_1-X_2 systems (where X_1 and X_2=Ni, Mo, Cr). Moreover, the high-throughput experimental technique used in this study has the potential to be applied to other materials systems and phase transformations, opening new avenues for research and discovery.

The obtained results demonstrate that a modified version of the ‘three-jump’ solute drag model can accurately predict ferrite growth kinetics in these systems, using only parameters derived from the ternary Fe-C-X_1 and Fe-C-X_2 alloys and Wagner interaction coefficients in austenite. This is attributed to the complete description of all the different interaction parameters of solutes with the moving interface (Fe-X and Fe-C) and between the different solutes within the interface (X-C and X_1-X_2). The present results highlight the importance of taking into account the individual binding energies of the different solutes to describe the complex interactions between solutes within the interface. The proposed approach was proven to be more effective in describing the growth kinetics than the initial version of the model that did not account for the different interactions, in systems where complex interaction behavior between solutes is expected, i.e. the

case of Fe-C-Ni-Mo.

While these findings represent a significant advancement in our understanding of ferrite growth kinetics in multi-component steels, further research is necessary to address questions related to the thermodynamic properties of the interface, including the carbon-interface interaction parameter and its dependency on temperature. Additionally, future studies can focus on the application of this model to non-isothermal ferrite precipitation in steel alloys, using the same high-throughput experimental technique.

Declaration of Competing Interest

The authors declare that they have no known competing financial interests or personal relationships that could have appeared to influence the work reported in this paper.

Acknowledgments

The authors extend their gratitude to DESY (located in Hamburg, Germany) for the access to their experimental facilities. They would also like to thank Dr. U. Lienert and Dr. Z. Hegedues for their help in using the P21.2 beamline at PETRA III. The authors also acknowledge Prof. H.S. Zurob for his engaging discussions and valuable input regarding solute drag modeling. Furthermore, they express their appreciation to Dr. Florence Robaut for her support in conducting EPMA measurements. This research was supported by ANR (Agence Nationale de la Recherche) [ANR-15-IDEX-02] and MIAI@Grenoble Alpes [ANR-19-P3IA-0003].

Supplementary materials

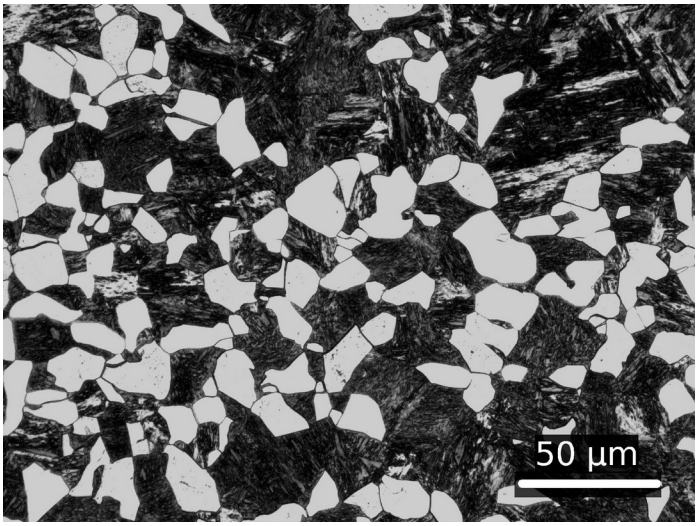

Figure S1: Optical micrograph showing the ferrite/martensite microstructure of a Fe-C-Ni-Mo diffusion couple transformed at 750 °C for 30s. Ferrite (in white) is formed along the prior austenite grain boundaries.

References

[1] H. K. D. H. Bhadeshia. Diffusional formation of ferrite in iron and its alloys. *Progress in Materials Science*, 29(4):321–386, January 1985.

[2] M. Gouné, F. Danoix, J. Ågren, Y. Bréchet, C.R. Hutchinson, M. Militzer, G. Purdy, S. van der Zwaag, and H. Zurob. Overview of the current issues in austenite to ferrite transformation and the role of migrating interfaces therein for low alloyed steels. *Materials Science and Engineering: R: Reports*, 92:1–38, June 2015.

[3] A. Van der Ven and L. Delaey. Models for precipitate growth during the $\gamma \rightarrow \alpha + \gamma$ transformation in Fe-C and Fe-C-M alloys. *Progress in Materials Science*, 40(3):181–264, January 1996.

[4] David A. Porter and Kenneth E. Easterling. *Phase transformations in metals and alloys*. Chapman & Hall, London, 2nd ed., reprinted edition, 1993. OCLC: 238829435.

[5] S. van der Zwaag. Kinetics of phase transformations in steels. In *Phase Transformations in Steels*, pages 126–156. Elsevier, 2012.

[6] M Hillert. Paraequilibrium. *Report of the Swedish Institute for Metal Research, Stockholm, Sweden*, 1953.

[7] Masato Enomoto. Comparison of alloy element partition behavior and growth kinetics of proeutectoid ferrite in Fe-C-X alloys with diffusion growth theory. *ISIJ Int.*, 28(10):826–835, 1988.

[8] J. B. Gilmour, G. R. Purdy, and J. S. Kirkaldy. Partition of manganese during the proeutectoid ferrite transformation in steel. *Metallurgical Transactions*, 3(12):3213–3222, December 1972.

[9] C. R. Hutchinson, H. S. Zurob, and Y. Bréchet. The growth of ferrite in Fe-C-X alloys: The role of thermodynamics, diffusion, and interfacial conditions. *Metallurgical and Materials Transactions A*, 37(6):1711–1720, June 2006.

[10] C. Qiu, H. S. Zurob, D. Panahi, Y. J. M. Brechet, G. R. Purdy, and C. R. Hutchinson. Quantifying the Solute Drag Effect on Ferrite Growth in Fe-C-X Alloys Using Controlled Decarburization Experiments. *Metallurgical and Materials Transactions A*, 44(8):3472–3483, August 2013.

[11] A. Béché, H.S. Zurob, and C.R. Hutchinson. Quantifying the Solute Drag Effect of Cr on Ferrite Growth Using Controlled Decarburization Experiments. *Metallurgical and Materials Transactions A*, 38(12):2950–2955, November 2007.

[12] I-E Benrabah, HP Van Landeghem, F Bonnet, B Denand, G Geandier, and A Deschamps. Solute drag modeling for ferrite growth kinetics during precipitation experiments. *Acta Materialia*, page 117364, 2021.

[13] Imed-Eddine Benrabah, Frédéric Bonnet, Benoît Denand, Alexis Deschamps, Guillaume Geandier, and Hugo P Van Landeghem. High-throughput compositional mapping of phase transformation kinetics in low-alloy steel. *Applied Materials Today*, 23:100997, 2021.

[14] C.W. Sinclair, C.R. Hutchinson, and Y. Bréchet. The Effect of Nb on the Recrystallization and Grain Growth of Ultra-High-Purity alpha-Fe: A Combinatorial Approach. *Metallurgical and Materials Transactions A*, 38(4):821–830, June 2007.

[15] Ernst Gamsjäger. A note on the contact conditions at migrating interfaces. *Acta materialia*, 55(14):4823–4833, 2007.

[16] John W Cahn. The impurity-drag effect in grain boundary motion. *Acta metallurgica*, 10(9):789–798, 1962.

[17] J. Odqvist, Mats Hillert, and John \AAgren. Effect of alloying elements on the γ to α transformation in steel. I. *Acta Materialia*, 50(12):3213– 3227, 2002.

[18] H. S. Zurob, D. Panahi, C. R. Hutchinson, Y. Brechet, and G. R. Purdy. Self-Consistent Model for Planar Ferrite Growth in Fe-C-X Alloys. *Metallurgical and Materials Transactions A*, 44(8):3456–3471, August 2013.

[19] Hao Chen, Kangying Zhu, Lie Zhao, and Sybrand van der Zwaag. Analysis of transformation stasis during the isothermal bainitic ferrite formation in Fe–C–Mn and Fe–C–Mn–Si alloys. *Acta Materialia*, 61(14):5458–5468, August 2013.

[20] I-E Benrabah, HP Van Landeghem, Frédéric Bonnet, Benoit Denand, Guillaume Geandier, and Alexis Deschamps. High-throughput investi- gation of ferrite growth kinetics in graded ternary fe-cx alloys. *Materialia*, 24:101480, 2022.

[21] H. I. Aaronson, W. T. Reynolds, and G. R. Purdy. Coupled-solute drag effects on ferrite formation in Fe-C-X systems. *Metallurgical and Materials Transactions A*, 35(4):1187–1210, April 2004.

[22] H. Guo, G. R. Purdy, M. Enomoto, and H. I. Aaronson. Kinetic transitions and substititional solute (Mn) fields associated with later stages of ferrite growth in Fe-C-Mn-Si. *Metallurgical and Materials Transactions A*, 37(6):1721–1729, June 2006.

[23] C. Qiu, H.S. Zurob, and C.R. Hutchinson. The coupled solute drag effect during ferrite growth in Fe–C–Mn–Si alloys using controlled decarburization. *Acta Materialia*, 100:333–343, November 2015.

[24] G. R. Purdy and Y. J. M. Brechet. A solute drag treatment of the effects of alloying elements on the rate of the proeutectoid ferrite transformation in steels. *Acta metallurgica et materialia*, 43(10):3763–3774, 1995.

[25] H. Guo and M. Enomoto. Effects of Substitutional Solute Accumulation at α/γ Boundaries on the Growth of Ferrite in Low Carbon Steels. *Metallurgical and Materials Transactions A*, 38(6):1152–1161, July 2007.

[26] F. Danoix, X. Sauvage, D. Huin, L. Germain, and M. Gouné. A direct evidence of solute interactions with a moving ferrite/austenite interface in a model Fe-C-Mn alloy. *Scripta Materialia*, 121:61–65, August 2016.

[27] W.W. Sun, H.S. Zurob, and C.R. Hutchinson. Coupled solute drag and transformation stasis during ferrite formation in Fe-C-Mn-Mo. *Acta Materialia*, 139:62–74, October 2017.

[28] Jérôme Kieffer and Dimitrios Karkoulis. Pyfai, a versatile library for azimuthal regrouping. In *J. Phys. Conf. Ser*, volume 425, page 36, 2013.

[29] Juan Rodriguez-Carvajal. Fullprof: a program for rietveld refinement and pattern matching analysis. In *satellite meeting on powder diffraction of the XV congress of the IUCr*, volume 127. Toulouse, 1990.

[30] Jan-Olof Andersson, Thomas Helander, Lars Höglund, Pingfang Shi, and Bo Sundman. Thermo-calc & dictra, computational tools for materials science. *Calphad*, 26(2):273–312, 2002.

[31] C. R. Hutchinson, A. Fuchsmann, and Y. Brechet. The diffusional formation of ferrite from austenite in Fe-C-Ni alloys. *Metallurgical and Materials Transactions A*, 35(4):1211–1221, April 2004.

[32] F. Fazeli and M. Militzer. Application of solute drag theory to model ferrite formation in multiphase steels. *Metallurgical and Materials Transactions A*, 36(6):1395–1405, June 2005.

[33] Ernst Gamsjäger, Robert E Werner, Wolfgang Schiller, and Bruno Buchmayr. Kinetics of the austenite-to-f errite phase transformation–simulations and experiments. *steel research international*, 85(2):131–142, 2014.

[34] Thermo-Calc Software - Computational Materials Engineering.